Eurasian Journal of Physics and Functional Materials

2026, 10(4), 376-398

Neutron scattering by clusters of the Carbon-12 nucleus

V.V. Lugovoi[1,*], K.G. Gulamov[1,**],
F.Kh. Ergashev[2], B.A. Sindarov[1]

[1]Physical-Technical Institute of the Academy of Sciences of the Republic of Uzbekistan

[2]Institute of Nuclear Physics of the Academy of Sciences of the Republic of Uzbekistan

E-mail: *lugovoi@uzsci.net, **gulamov@uzsci.net

DOI: **10.32523/ejpfm.2026100404**
Received: 16 October 2026
Revised: 05 November 2026
Accepted: 14 November 2026

Above the Hoyle resonance, the excited states of the ^{12}C nucleus begin to overlap strongly. To separate them, various theoretical models are used, which predict different spectra of angular distributions of the decay products (α -particles). This leads to discrepancies of 30–50% or more in cross-section estimates in the ENDF, JEFF, and JENDL nuclear databases. In this work, we investigate the hypothesis of a possible connection between the population of resonant states of the ^{12}C nucleus and the scattering of a projectile neutron on various clusters of the ^{12}C nucleus with a 3α or $\alpha - {}^{8}Be$ structure. For this purpose, the interaction of 14 MeV neutrons with a stationary ^{12}C nucleus was investigated, where within a nuclear potential well of depth 45 MeV and width $L \sim 5$ fm, the de Broglie wavelength of the incident neutron ($\lambda_n \approx 0.58$ fm) allows it to spatially resolve intranuclear α -clusters ($\lambda_\alpha \sim 1.68$ fm). Therefore, as a first rough approximation, independent quantum scattering of a neutron off the ^{12}C nuclear clusters is modeled in momentum-energy representation, leading to nuclear excitation. To this end, the partial differential cross sections for $n\alpha$ and $n - {}^{8}Be$ scattering were adopted from the phenomenological phase-shift analysis at IAEA EXFOR Database. Monte Carlo simulations allowed us to calculate the mass-energy distribution of the excited $^{12}C^*$ nucleus and make a comparison with experimental population probabilities for the excited $^{12}C^*$. Despite the rough approximation of cluster independence, qualitative consistency is observed. A strong discrepancy occurs at points where strict quantum suppression or nuclear collectivity is strongly dominant. For neutron scattering on different cluster structures, the model predicts different population probabilities for the excited $^{12}C^*$, which indicates the need for further calculations within a more realistic model that strictly accounts for the overlap of the de Broglie waves of the α -particles.

Keywords: Monte Carlo; neutron; carbon resonance states; clustered structure.

1. Introduction

The hypothesis that heavier nuclei contain clusters with the nucleon composition of lighter nuclei, along with the tendency of nucleons to combine into various cluster configurations [1–8], has long attracted attention. This concept may prove highly useful, for example, for solving the problem of controlled thermonuclear fusion of heavier nuclei from lighter ones. Controlling such nuclear processes requires detailed knowledge of cluster properties, which, however, can vary significantly in their nucleon structure.

In Ref. [9], a fundamental review on the cluster structure of nuclei is presented. In studying nuclear clustering, a specific yet important subject of research is the reaction at thermonuclear fusion energy, where, however, knowledge of the cluster configuration (primarily the α-cluster structure) in the $^{12}\mathrm{C} + n \to n' + 3\alpha$ reactions at a neutron energy of about 14 MeV is not strictly unambiguous. For instance, in the region of overlapping resonances, it is impossible to unambiguously assign α-particles to a specific resonance. Therefore, theoretical predictions for angular and momentum spectra are used to separate the particles. Consequently, knowledge of the cluster configuration in these reactions is probabilistic and model-dependent. The model parameters depend on the set of experiments that the model aims to describe. Over time, this leads to uncertainties in the determination of cross sections. In [10], a comparison is made between data from global nuclear data libraries (ENDF/B-VIII.0, JEFF-3.3, etc.) and experimental data. It is shown that for peaks corresponding to the formation of intermediate particles, the discrepancies range from 35% to 50% or more, depending on the chosen library.

To find a way to overcome this problem, this work attempts to investigate a possible relationship between the population level distribution of resonant states and the scattering of a 14-MeV neutron on two different clusterizations of the $^{12}\mathrm{C}$ nucleus (3α or $\alpha - {}^{8}\mathrm{Be}$). Such a dependence could shed light on the potential connection between cross sections and the cluster structure.

When moving in a vacuum with a kinetic energy $E_{\mathrm{kin}} = 14$ MeV and a corresponding momentum $p = k\hbar$, the size of the neutron wave packet is characterized by its de Broglie wavelength $\lambda = \frac{h}{p} = 7.65$ fm. When describing the nuclear interaction, this same neutron is characterized by a smaller wavelength, $\bar{\lambda} = \frac{\lambda}{2\pi} = 1.2$ fm (see Chapter VIII, "Nuclear Reactions: General Theory," in [11]), which sets the scale of nuclear interactions. Upon entering the nuclear potential well, the wavelength of the neutron decreases even further. This is due to the fact that nucleons in the nucleus obey the Pauli exclusion principle and form a quantum Fermi gas. The depth of the potential well, V_0, is the sum of the Fermi energy ($E_F \approx 37$ MeV for nuclear matter) and the average nucleon binding energy ε ($\varepsilon \approx 8$ MeV). Thus, we have $V_0 = E_F + \varepsilon = 45$ MeV. Within the framework of the optical model of the nucleus [12], this value of V_0 helps accurately reproduce experimental elastic scattering and absorption cross sections, representing the minimum required depth to bind nucleons inside the nucleus while accounting for their internal kinetic motion. Therefore, our model adopts the optical model parameters [13] as discussed below.

As a neutron transitions from vacuum into the nucleus, its potential energy decreases by the depth of the potential well, V_0. According to the law of conservation of energy, this leads to an increase in its kinetic energy from E_{kin} to $E'_{\text{kin}} = E_{\text{kin}} + V_0 = 14\ \text{MeV} + 45\ \text{MeV} = 59\ \text{MeV}$. This increase in kinetic energy results in a higher nucleon momentum, which can be defined in terms of the neutron mass $m_n = 939.57\ \text{MeV}$ via the non-relativistic relation $p = \sqrt{2m_n(E_{\text{kin}} + V_0)}$. Consequently, in accordance with the de Broglie hypothesis, the reduced wavelength of the neutron inside the nuclear medium is given by $\lambda^n_{\text{de Broglie}} = \frac{\hbar}{\sqrt{2m_n(E_{\text{kin}}+V_0)}} = 0.58\ \text{fm}$. Note that such a change in wavelength is equivalent to the refraction of waves in optics, which serves as the fundamental basis for calculating scattering cross sections in Refs. [14, 15].

A comparison of this value, $\lambda^n_{\text{de Broglie}} = 0.58\ \text{fm}$, with the size of the α-particle, $\lambda^\alpha_{\text{de Broglie}} = 1.68\ \text{fm}$ [16], indicates that inside an unexcited ^{12}C nucleus (with a diameter of $L \approx 5\ \text{fm}$ [17]), the projectile neutron is capable of resolving an individual α-particle and can thus undergo quantum-mechanical scattering on it.

However, these figures show that the ratio of the nuclear volume to the volume of an α-particle is ≈ 3.2. This shows that the wave functions of the α-particles constituting the ^{12}C nucleus overlap, and considering their motion as independent would be a rough approximation. Strictly speaking, it would therefore not be entirely accurate to treat quantum $n-\alpha$ scatterings on two α-particles within the same nucleus as independent processes. However, in nuclear matter, the mean free path for a 14 MeV nucleon is approximately 2–4 fm, which is comparable to the size of the ^{12}C nucleus itself [11]. Consequently, the interaction of a 14 MeV neutron with the ^{12}C nucleus exhibits the character of a direct nuclear reaction (or fast elastic/inelastic scattering) or a pre-equilibrium process [18]. Furthermore, the velocity of the high-energy quasiclassical neutron is approximately 13 times greater than the Fermi motion velocity of the α-cluster; this implies that, kinematically, a response involving the entire cluster structure of the ^{12}C nucleus can occur (with a non-zero probability) only after the neutron has exited the nucleus. In addition, as a ^{4}He-like structure, the α-cluster represents a nucleon structure with the strongest binding energy, meaning that the energy required to remove nucleons from the α-cluster exceeds the capabilities of the projectile neutron, which must already spend 45 MeV to escape the nucleus. On this basis, as a rough first-order approximation, let us consider the above-mentioned independent quantum $n-\alpha$ scattering on one, two, and three α-clusters or on the ^{8}Be nucleus.

In other words, let us formulate and test the hypothesis that during the elastic "probing" of nuclear matter structures at low energies, the neutron–owing to its lack of Coulomb charge–possesses unique properties analogous to those of X-rays used to study molecular structures. The present research is based on this concept.

The fundamental property of the ^{4}He nucleus to have the highest nucleon binding energy is not only the cause of the alpha-cluster structure of the carbon-12 nucleus, but also the reason for the formation of the ^{12}C nucleus itself, when threshold values for cluster states arise [6], which allows excitation energy to

transform into binding energy [7]. Thus, the occurrence of excitation states in ^{12}C nuclei is related to fundamental issues of nuclear physics. This paper proposes a mechanism for the generation of excited states of the ^{12}C nucleus in neutron–carbon-12 scattering reactions at energies around 14 MeV, that is, below the threshold for the possible disintegration of the ^{4}He cluster [8].

In $n-^{12}$C scattering, several variants of the ^{12}C cluster structure are possible, namely those consisting of three alpha particles, an alpha particle and an ^{8}Be nucleus, as well as the least probable (up to 26 MeV) (^{3}He $+^{9}$ Be) structure [8]. Therefore, we will consider the most probable cluster structures (^{4}He $+^{8}$ Be) and (^{4}He $+^{4}$ He $+^{4}$ He).

Based on these considerations, in this paper we propose a semi-classical mechanism for the formation of the excited state of the ^{12}C nucleus, viewing it as a cluster system composed of ^{8}Be and ^{4}He nuclei. Specifically, we analyze four elastic scattering channels. The first channel involves single elastic scattering of a 14-MeV neutron on an intra-nuclear ^{4}He cluster. The second channel describes a cascade scattering sequence, where the neutron scatters first on the ^{4}He cluster and subsequently on the ^{8}Be cluster. This is for the first cluster structure (^{4}He $+^{8}$ Be). For the second cluster structure (^{4}He $+^{4}$ He $+^{4}$ He), we consider channels of sequential neutron scattering on two and three ^{4}He clusters. Note that in Monte Carlo codes such as SCINFUL [19] and GEANT4 [20], an effective quasi-free approximation is frequently employed at low energies. In our model, this approach can be formulated as the assumption that in the interaction act, the neutron transfers momentum to a local cluster, while the remaining part of the nucleus acts as a spectator.

In this case, for neutron–cluster scattering, one can use the distributions presented in Figures 1 and 2, while strictly taking into account the Fermi motion of the cluster inside the carbon nucleus. As noted in [13], precise phase-shift data for the $n-^{4}$He system is critical for testing few-nucleon interaction models, spin–orbit interactions, and three-nucleon forces in light nuclear systems.

Therefore, to calculate the scattering angles in the $n+\alpha$ center-of-mass system, let us use Figure 1, where differential cross sections for elastic neutron–α scattering in the center-of-mass (c.m.) frame for incident neutron energies in the potential well of the resting ^{12}C nucleus ranging from $E_n = 45$ to 70 MeV were evaluated using the global phase-shift parameterization [13, 21–23] alongside available experimental datasets from the EXFOR library [24].

In accordance with the diffraction multiple scattering theory for two-center cluster targets [25, 26], the differential cross section $\frac{d\sigma}{d\Omega}_{n-^{8}\mathrm{Be}}$ can be factorized into the constituent $n-\alpha$ cross section and the spatial interference factor averaged over the isotropic orientation of the 2α-system [27, 28]:

$$\left(\frac{d\sigma}{d\Omega}\right)_{n-^{8}\mathrm{Be}}(\theta_{\mathrm{c.m.s.}}) \approx 2\left[1+\frac{\sin(qR_{\alpha\alpha})}{qR_{\alpha\alpha}}\right]\cdot\left(\frac{d\sigma}{d\Omega}\right)_{n\alpha}(\theta_{\mathrm{c.m.s.}}).$$

Here the vector $\vec{q}=\vec{k}-\vec{k}'$, where $\vec{k}$ and $\vec{k}'$ are the wave vectors of the incident and scattered neutron in the center-of-mass system (c.m.s.). The magnitude of this vector $|\vec{q}| = 2k\sin\left(\frac{\theta_{\mathrm{c.m.s.}}}{2}\right)$, indicates the momentum transferred by the scattered

neutron to the target nucleus upon deflection by an angle $\theta_{\text{c.m.s.}}$, provided that the wavenumber k of the incident neutron in the center-of-mass frame is equal to $k = \frac{\sqrt{2m_n E_{\text{c.m.s.}}}}{\hbar}$; $\vec{R}_{\alpha\alpha}$ is the intercluster distance vector, i.e., the magnitude $|\vec{R}_{\alpha\alpha}| = R_{\alpha\alpha} \approx 3.4$ fm, is the average spatial distance between clusters in the 2α structure of the ^{8}Be nucleus. In the 0^+ ground state of the ^{8}Be nucleus, the vector $\vec{R}_{\alpha\alpha}$ is isotropically oriented relative to the transferred momentum vector $\vec{q}$. Thus, a relationship arises between $\theta_{\text{c.m.s.}}$ and $E_{\text{c.m.s.}}$, and the values presented in Figure 2 are calculated.

Such a factorization has the following explanation [27, 28]. Because the α-particle is a spin-zero boson ($J^\pi = 0^+$), the elastic $n-\alpha$ scattering amplitude is free from target spin-orientation degrees of freedom. As a result, the two constituent α-clusters in the ^{8}Be nucleus ($J^\pi = 0^+$) do not introduce spin-flip interference or spin-statistical weighting coefficients. Consequently, the spin-orbit interactions are fully encapsulated within the individual unpolarized differential cross section $\left(\frac{d\sigma}{d\Omega}\right)_{n\alpha}$, allowing the spatial interference factor $2\left[1+\frac{\sin(qR_{\alpha\alpha})}{qR_{\alpha\alpha}}\right]$ to factorize completely as a scalar multiplier.

The nuclear data presented in IAEA demonstrate that these scattering angle distributions exhibit a distinct energy dependence. On the other hand, we can calculate the excited mass distributions of the ^{12}C nucleus for each fixed incident neutron energy and for each fixed nucleon composition of the cluster. This makes it possible to separate the experimental ($n-^{12}$C) events according to the type of cluster structure manifested in these events with a sufficiently high degree of reliability. Details are presented in the following sections.

Let us note that there is a well-known formula (see Eqs. (7.1)–(7.2) in [29] or Eq. (3.28) in [30]) for the dependence of the fraction of energy $\frac{E_A}{E_n} = \left[1-\frac{\left(\cos\theta+\sqrt{A^2-\sin^2\theta}\right)^2}{(A+1)^2}\right]$ transferred by a neutron n with kinetic energy E_n to a nucleus with mass number A (in our case, to a nuclear cluster with A nucleons) during elastic neutron scattering through an angle θ in the nucleus rest frame. At $\theta = 0^\circ$, this fraction is $\frac{E_A}{E_n} = 0$, while at $\theta = \pi$, the ratio $\frac{E_A}{E_n}$ takes its maximum value equal to $\frac{4A}{(A+1)^2}$. Thus, in elastic neutron–cluster scattering, the neutron can transfer various fractions of its energy, thereby exciting the carbon nucleus as a whole. According to the given formula, the fraction of energy transferred by the neutron depends on the number of nucleons A in the cluster and on the scattering angle θ. Consequently, the excitation energy of the ^{12}C nucleus will also have a similar dependence. In our study, we will not use the formula given above. Instead, in each Monte Carlo event, we will generate the elastic neutron–cluster scattering angle in their center-of-mass system, and in accordance with Figures 1 or 2, where the scattering angle is defined relative to the z axis aligned with the neutron momentum prior to its scattering on the cluster.

The algorithm of our Monte Carlo model and a discussion of the results are presented in the following sections.

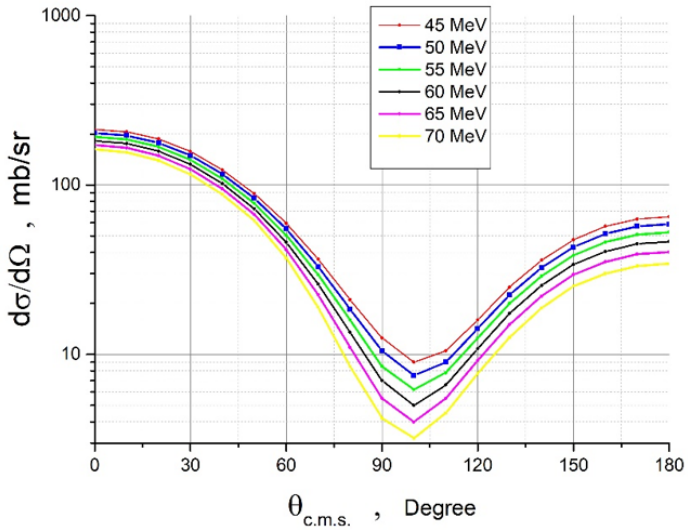


Figure 1. Theoretical calculation of the differential elastic $neutron-\alpha$ scattering cross section in the $n+\alpha$ center-of-mass system for various neutron energies in the potential well of the resting ^{12}C nucleus. The data were obtained from phase-shift analysis [13, 21–23] and digitized IAEA EXFOR database sets (Entry 22312) [24].

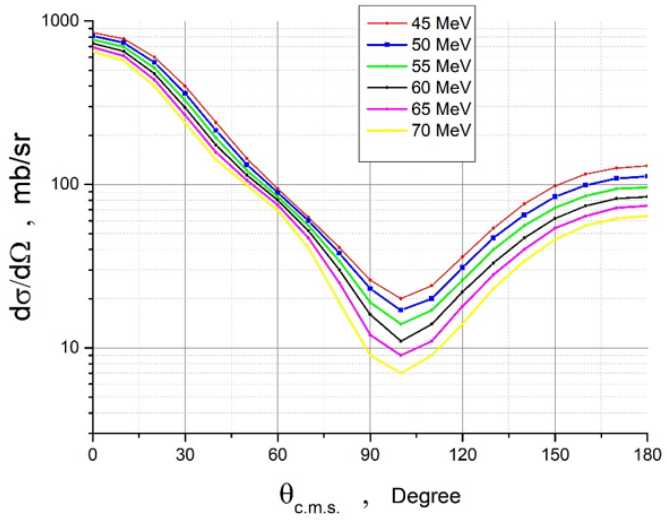


Figure 2. Theoretical calculation of the differential elastic neutron–^{8}Be scattering cross section in the $n+^{8}$Be center-of-mass system for various neutron energies in the potential well of the resting ^{12}C nucleus (see Sect. 1, Refs. [13, 21–28]).

2. Neutron scattering on a single cluster

2.1 Monte Carlo algorithm

In this paper, we test a hypothesis about the proposed mechanism for the formation of the excited ^{12}C nucleus with two possible clusterings ($^{4}He+^{8}Be$) and ($^{4}He+^{4}He+^{4}He$). First, let us consider the $^{4}He+^{8}Be$ clustering. The excitation is believed to be caused by elastic scattering of a neutron with a kinetic energy of 14 MeV on ^{4}He and ^{8}Be clusters, whose momenta, in the ground state of the ^{12}C nucleus, are distributed isotropically and have mutually opposite directions in the rest frame of ^{12}C.

In the experimental study [31], the intrinsic momentum distribution of α-clusters in the ground state of the ^{12}C nucleus was directly reconstructed from

proton-induced cluster knockout reactions using both direct measurements and the distorted-wave impulse approximation (DWIA), yielding a width for their momentum distribution of $\bar{p} \approx (110-130)$ MeV/c. Therefore, to ensure the required isotropy in the ^{12}C rest frame (which coincides with the laboratory frame K_L), the x, y, and z components of the ^{4}He cluster momentum were generated according to a Gaussian distribution with the parameter $\sigma = \sqrt{\pi/2}\,\bar{p}$, where $\bar{p} = 100$ MeV/c, using the formula:

$$p^{\text{Lab}}_{\text{He}\,x(y,z)} = \cos(2\pi r_1) \cdot \sqrt{-2\log(r_2)} \cdot \sigma, \tag{1}$$

where r_1, r_2 are random numbers uniformly distributed in the interval $(0,1)$. In the same K_L frame, the projections of the ^{8}Be cluster momentum and the energies of the ^{4}He and ^{8}Be clusters were determined using the formulas

$$p^{\text{Lab}}_{\text{Be}\,x(y,z)} = -\,p^{\text{Lab}}_{\text{He}\,x(y,z)}, \tag{2}$$

$$E_{\text{He}} = \sqrt{m^2_{^4\text{He}} + \left(p^{\text{Lab}}_{\text{He}\,x}\right)^2 + \left(p^{\text{Lab}}_{\text{He}\,y}\right)^2 + \left(p^{\text{Lab}}_{\text{He}\,z}\right)^2}, \qquad E_{\text{Be}} = M^0_{^{12}\text{C}} - E_{\text{He}}, \tag{3}$$

where the masses of the ^{4}He cluster and the ^{12}C ground state were taken as $m_{^4\text{He}} = 3727.3794$ MeV and $M^0_{^{12}\text{C}} = 11174.862$ MeV, respectively. Thus, only the ^{4}He cluster was assumed to be on the mass shell.

As shown in Sect. 1, inside the potential well of the resting ^{12}C nucleus, the incident neutron has an energy $(E_{\text{kin}} + V_0) = 59$ MeV and a momentum $\left|\vec{p}^{\,\text{Lab}}_n\right| = \sqrt{2m_n(E_{\text{kin}} + V_0)} = 333$ MeV/c .This projectile neutron penetrates into the nucleus due to nuclear attractive forces; that is, to a good approximation, it enters the nucleus perpendicular to the nuclear surface without changing its direction. Therefore, the transverse x, y components of the momentum $\vec{p}^{\,\text{Lab}}_n$ are equal to zero, and the longitudinal component was found by the formula $p^{\text{Lab}}_{n,z} = \left|\vec{p}^{\,\text{Lab}}_n\right|$.

The center-of-mass system (n - ^{4}He) moves in the laboratory coordinate system with momentum

$$\vec{p}^{\,\text{Lab}}_{n-\text{He}} = \vec{p}^{\,\text{Lab}}_n + \vec{p}^{\,\text{Lab}}_{\text{He}}. \tag{4}$$

Therefore, to move from K_L to the ($n +^4$ He) center-of-mass system, we turn the K_L system, directing the z^* axis along to the momentum $\vec{p}^{\,\text{Lab}}_{n-\text{He}}$, and the y^* axis along to the vector product $\vec{z}^{\,*} \times \vec{z}_L$. We define this new system as K^*. The rotation angles φ, θ from K_L to K^* (and back) are determined by the following relations:

$$\cos\varphi = \frac{-p^{x\,\text{Lab}}_{n-\text{He}}}{\sqrt{\left(p^{x\,\text{Lab}}_{n-\text{He}}\right)^2 + \left(p^{y\,\text{Lab}}_{n-\text{He}}\right)^2}}, \qquad \sin\varphi = \frac{-p^{y\,\text{Lab}}_{n-\text{He}}}{\sqrt{\left(p^{x\,\text{Lab}}_{n-\text{He}}\right)^2 + \left(p^{y\,\text{Lab}}_{n-\text{He}}\right)^2}},$$

$$\cos\theta = \frac{-p^{z\,\mathrm{Lab}}_{n-\mathrm{He}}}{\sqrt{\left(p^{x\,\mathrm{Lab}}_{n-\mathrm{He}}\right)^2 + \left(p^{y\,\mathrm{Lab}}_{n-\mathrm{He}}\right)^2 + \left(p^{z\,\mathrm{Lab}}_{n-\mathrm{He}}\right)^2}}, \qquad \sin\theta = \sqrt{1-(\cos\theta)^2}. \quad (5)$$

Now the components of the neutron momentum in K^* can be expressed in terms of its components in K_L:

$$p^{x^*}_n = -\,p^{x\,\mathrm{Lab}}_n \cos\theta\cos\varphi - \,p^{y\,\mathrm{Lab}}_n \cos\theta\sin\varphi + \,p^{z\,\mathrm{Lab}}_n \sin\theta,$$

$$p^{y^*}_n = -\,p^{x\,\mathrm{Lab}}_n \sin\varphi + \,p^{y\,\mathrm{Lab}}_n \cos\varphi, \quad (6)$$

$$p^{z^*}_n = -\,p^{x\,\mathrm{Lab}}_n \sin\theta\cos\varphi - \,p^{y\,\mathrm{Lab}}_n \sin\theta\sin\varphi - \,p^{z\,\mathrm{Lab}}_n \cos\theta.$$

Next, let this K^* system move along the z^* axis with velocity (see (3), (4)) and Lorentz factor

$$\vec{\beta}_L = \frac{\vec{p}^{\,\mathrm{Lab}}_{n-\mathrm{He}}}{E_n + E_{\mathrm{He}}}, \qquad \gamma_L = \frac{1}{\sqrt{1-\beta_L^2}}, \quad (7)$$

where $E_n = E^{\mathrm{kin}}_n + m_n$ is the relativistic energy of the neutron and $m_n = 939.57$ MeV is the mass of the neutron.

Thus, we obtain the K' center-of-mass system of the neutron n and the ^{4}He cluster. Considering that the energy of the particles does not change under a rotation of the coordinate system, we can calculate the components of the momentum $\vec{p}\,'_n$ and the energy of the neutron n in this K' system using the following formulas ($|\vec{\beta}_L| = \beta_L$):

$$\begin{aligned} &p^{x'}_n = p^{x*}_n, \qquad p^{y'}_n = p^{y*}_n, \qquad p^{z'}_n = \gamma_L\left(p^{z*}_n - \beta_L E_n\right), \\ &E'_n = \sqrt{m_n^2 + (p^{x'}_n)^2 + (p^{y'}_n)^2 + (p^{z'}_n)^2}. \end{aligned} \quad (8)$$

However, the direction of the x, y, z coordinate axes in K' does not coincide with the direction of the coordinate axes used in [21–24] to obtain the required distributions shown in Figure 1, where the scattering angles are given relative to the z axis, which is chosen along the neutron momentum before its elastic scattering on the ^{4}He nucleus. Therefore, it is necessary to rotate the K' system so as to obtain the z'^* axis along the momentum vector $\vec{p}\,'_n$, and the y'^* axis along the vector product $\vec{z}\,'^* \times \vec{z}\,'$. We define this new system as K'^*. The K'^* system completely coincides with the experimental system in which the data in Figure 1 are presented.

Let us determine the angles φ', θ' of rotation from the K' system to the K'^* system (and back):

$$\cos\varphi' = \frac{-p_n^{x'}}{\sqrt{(p_n^{x'})^2 + (p_n^{y'})^2}},$$

$$\sin\varphi' = \frac{-p_n^{y'}}{\sqrt{(p_n^{x'})^2 + (p_n^{y'})^2}},$$

$$\cos\theta' = \frac{-p_n^{z'}}{\sqrt{(p_n^{x'})^2 + (p_n^{y'})^2 + (p_n^{z'})^2}}, \tag{9}$$

$$\sin\theta' = \sqrt{1 - (\cos\theta')^2}.$$

Now, in the K'^* frame, the neutron scattering angle $\theta_{n-\mathrm{He}}^{\mathrm{c.m.s.}}$ is generated randomly according to the distributions shown in Figure 1, where out of eight distributions, the one whose energy is closest to the neutron energy equal to $(E_{\mathrm{kin}} + V_0)$ was selected. For the first neutron–cluster scattering, this condition is satisfied by the distribution corresponding to an energy of 60 MeV, since $(E_{\mathrm{kin}} + V_0) = 59$ MeV. In Sections 3, 4, and 5, a cascade of neutron scatterings on clusters is considered, where the energy of the elastically scattered neutron can randomly decrease or increase. However, each time, the angle $\theta_{n-\mathrm{He}}^{\mathrm{c.m.s.}}$ was generated according to one of the distributions (Figure 1 or Figure 2) selected by the same principle.

Assuming symmetry in the azimuthal plane, the azimuthal angle $\varphi_{n-\mathrm{He}}^{\mathrm{c.m.s.}}$ is generated isotropically by a random number r_3, uniformly distributed over the interval $(0, 1)$:

$$\varphi_{n-\mathrm{He}}^{\mathrm{c.m.s.}} = 2\pi r_3. \tag{10}$$

The momentum vectors of the neutron and the cluster, both before and after the elastic interaction, are equal in magnitude and opposite in direction in their center-of-mass system. Following the elastic scattering, the neutron momentum vector retains its magnitude but changes its direction according to the distribution shown in Figure 1. This leads to a modification of the initial momenta and energies of the neutron and the cluster in the laboratory frame. This sequence of Lorentz transformations and coordinate system rotations–wherein the "mixing" (12)–(13) of the post-scattering momentum components (11) takes place–is the primary cause of the change in the initial kinematic values in the laboratory frame. This is precisely what occurs in our calculation. Here, let us recall that the relationship between the elastic scattering angle and the energies of the neutron and a free nucleus with atomic mass number A has long been well established experimentally (see [29, 30]).

Thus, in the center-of-mass system K'^* after scattering, the neutron n' and cluster $^4\mathrm{He}'$ have components $(|\vec{p}_n''| = |\vec{p}_n'|)$:

$$p_{n'}^{x'^*} = \left|\vec{p}_n'\right| \cos\left(\varphi_{n-\mathrm{He}}^{\mathrm{c.m.s.}}\right) \sin\left(\theta_{n-\mathrm{He}}^{\mathrm{c.m.s.}}\right),$$

$$p_{n'}^{y'^*} = \left|\vec{p}_n'\right| \sin\left(\varphi_{n-\mathrm{He}}^{\mathrm{c.m.s.}}\right) \sin\left(\theta_{n-\mathrm{He}}^{\mathrm{c.m.s.}}\right),$$

$$p_{n'}^{z'^*} = \left|\vec{p}_n'\right| \cos\left(\theta_{n-\mathrm{He}}^{\mathrm{c.m.s.}}\right), \tag{11}$$

$$p_{\mathrm{He}'}^{x'^*} = -p_{n'}^{x'^*}, \qquad p_{\mathrm{He}'}^{y'^*} = -p_{n'}^{y'^*}, \qquad p_{\mathrm{He}'}^{z'^*} = -p_{n'}^{z'^*},$$

which, in the K' system, take the form (see (9)) for the neutron:

$$p_{n'}^{x'} = -\,p_{n'}^{x'^*}\cos\theta'\cos\varphi' - \,p_{n'}^{y'^*}\sin\varphi' - \,p_{n'}^{z'^*}\sin\theta'\cos\varphi',$$

$$p_{n'}^{y'} = -\,p_{n'}^{x'^*}\cos\theta'\sin\varphi' + \,p_{n'}^{y'^*}\cos\varphi' - \,p_{n'}^{z'^*}\sin\theta'\sin\varphi', \tag{12}$$

$$p_{n'}^{z'} = p_{n'}^{x'^*}\sin\theta' - p_{n'}^{z'^*}\cos\theta';$$

and for the scattered He' cluster:

$$p_{\mathrm{He}'}^{x'} = -\,p_{\mathrm{He}'}^{x'^*}\cos\theta'\cos\varphi' - \,p_{\mathrm{He}'}^{y'^*}\sin\varphi' - \,p_{\mathrm{He}'}^{z'^*}\sin\theta'\cos\varphi',$$

$$p_{\mathrm{He}'}^{y'} = -\,p_{\mathrm{He}'}^{x'^*}\cos\theta'\sin\varphi' + \,p_{\mathrm{He}'}^{y'^*}\cos\varphi' - \,p_{\mathrm{He}'}^{z'^*}\sin\theta'\sin\varphi', \tag{13}$$

$$p_{\mathrm{He}'}^{z'} = p_{\mathrm{He}'}^{x'^*}\sin\theta' - p_{\mathrm{He}'}^{z'^*}\cos\theta'.$$

After calculating the energies n' and He'

$$E_{n'}' = \sqrt{\left(p_{n'}^{x'}\right)^2 + \left(p_{n'}^{y'}\right)^2 + \left(p_{n'}^{z'}\right)^2 + m_n^2},$$

$$E_{\mathrm{He}'}' = \sqrt{\left(p_{\mathrm{He}'}^{x'}\right)^2 + \left(p_{\mathrm{He}'}^{y'}\right)^2 + \left(p_{\mathrm{He}'}^{z'}\right)^2 + m_{^4\mathrm{He}}^2}. \tag{14}$$

Their momenta and energies were transformed from the K' system to the K^* system:

$$p_{n'}^{x^*} = p_{n'}^{x'}, \qquad p_{n'}^{y^*} = p_{n'}^{y'}, \qquad p_{n'}^{z^*} = \gamma_L\left(p_{n'}^{z'} + \beta_L E_{n'}'\right),$$

$$p_{\mathrm{He}'}^{x^*} = p_{\mathrm{He}'}^{x'}, \qquad p_{\mathrm{He}'}^{y^*} = p_{\mathrm{He}'}^{y'}, \qquad p_{\mathrm{He}'}^{z^*} = \gamma_L\left(p_{\mathrm{He}'}^{z'} + \beta_L E_{\mathrm{He}'}'\right). \tag{15}$$

and then from the K^* system to the laboratory K_L system

$$p_{n'}^{x\,\mathrm{Lab}} = -\,p_{n'}^{x^*}\cos\theta'\cos\varphi' - \,p_{n'}^{y^*}\sin\varphi' - \,p_{n'}^{z^*}\sin\theta'\cos\varphi',$$

$$p_{n'}^{y\,\mathrm{Lab}} = -\,p_{n'}^{x^*}\cos\theta'\sin\varphi' + \,p_{n'}^{y^*}\cos\varphi' - \,p_{n'}^{z^*}\sin\theta'\sin\varphi',$$

$$p_{n'}^{z\,\mathrm{Lab}} = p_{n'}^{x^*}\sin\theta' - p_{n'}^{z^*}\cos\theta',$$

$$p_{\mathrm{He}'}^{x\,\mathrm{Lab}} = -\,p_{\mathrm{He}'}^{x^*}\cos\theta'\cos\varphi' - \,p_{\mathrm{He}'}^{y^*}\sin\varphi' - \,p_{\mathrm{He}'}^{z^*}\sin\theta'\cos\varphi',$$

$$p_{\mathrm{He}'}^{y\,\mathrm{Lab}} = -\,p_{\mathrm{He}'}^{x^*}\cos\theta'\sin\varphi' + \,p_{\mathrm{He}'}^{y^*}\cos\varphi' - \,p_{\mathrm{He}'}^{z^*}\sin\theta'\sin\varphi',$$

$$p_{\mathrm{He}'}^{z\,\mathrm{Lab}} = p_{\mathrm{He}'}^{x^*}\sin\theta' - p_{\mathrm{He}'}^{z^*}\cos\theta'. \tag{16}$$

After calculating the energy of the $^4\mathrm{He}'$ cluster in the laboratory system,

$$E_{\mathrm{He}'}^{\mathrm{Lab}} = \sqrt{m_{^4\mathrm{He}}^2 + \left(p_{\mathrm{He}'}^{x\,\mathrm{Lab}}\right)^2 + \left(p_{\mathrm{He}'}^{y\,\mathrm{Lab}}\right)^2 + \left(p_{\mathrm{He}'}^{z\,\mathrm{Lab}}\right)^2}, \tag{17}$$

the energy of the excited nucleus in the same system was determined (see (3)):

$$E_{^{12}\mathrm{C}}^{*\,\mathrm{Lab}} = E_{^4\mathrm{He}'}^{\mathrm{Lab}} + E_{\mathrm{Be}}, \tag{18}$$

as well as its momentum:

$$\vec{p}_{^{12}\mathrm{C}}^{\,\mathrm{Lab}} = \vec{p}_n^{\,\mathrm{Lab}} - \vec{p}_{n'}^{\,\mathrm{Lab}}, \tag{19}$$

and mass

$$M_{^{12}\mathrm{C}}^{*} = \sqrt{\left(E_{^{12}\mathrm{C}}^{*\,\mathrm{Lab}}\right)^2 - \left(\vec{p}_{^{12}\mathrm{C}}^{\,\mathrm{Lab}}\right)^2}. \tag{20}$$

The fulfillment of the law of conservation of momentum follows from (19). To verify the law of conservation of energy, the value

$$\Psi = \left| \frac{\left(E_{^{12}\mathrm{C}}^{*\,\mathrm{Lab}} + E_{n'}^{\mathrm{Lab}}\right) - \left(M_{^{12}\mathrm{C}}^{0} + E_n^{\mathrm{Lab}}\right)}{M_{^{12}\mathrm{C}}^{0} + E_n^{\mathrm{Lab}}} \right|, \tag{21}$$

was calculated for each event. Here, $E_n^{\mathrm{Lab}} \equiv E_n$ is the relativistic energy of the neutron n (see (7)), $E_{n'}^{\mathrm{Lab}} = \sqrt{m_n^2 + \left(\vec{p}_{n'}^{\,\mathrm{Lab}}\right)^2}$ is the relativistic energy of the neutron that has been scattered by the $^4\mathrm{He}$ cluster.

In our study, we attempt to estimate the mass change of the $^{12}\mathrm{C}$ nucleus traversed by the neutron, which implies that the interaction must not change the particle species or their total number. In this case, to be able to leave the potential well of the nucleus with a depth of $V_0 = 45$ MeV (see Section 1), the scattered neutron must have an energy $E_{n'}^{\mathrm{Lab}} > 45$ MeV. Therefore, a Monte Carlo event was rejected if this inequality was not satisfied.

As can be seen from the algorithm described above, the calculations alternately perform Lorentz transformations (see (8), (15)) and three-dimensional coordinate system rotations (see (6), (12), (13), (16)), where the calculation of each momentum component in the rotated system involves all momentum components from the unrotated coordinate system. Therefore, in the case of an incorrect implementation within the Fortran code, such a complex entanglement of calculations leads to a sharp increase in the value of (21), which is sensitive to errors—that is, to a

deviation from the algorithm described above. Conversely, correct execution of the calculations results in a value of (21) corresponding to machine precision.

In all 10^6 simulated Monte Carlo events, the inequality

$$\Psi < 10^{-10}. \tag{22}$$

was satisfied, which demonstrates the high accuracy of energy and momentum conservation (see (19)) in the simulation of the $n + {}^{12}\mathrm{C} \to n' + {}^{12}\mathrm{C}^*$ process (see (23)) involving both Lorentz transformations and three-dimensional spatial rotations.

2.2 Results

In order to take into account all states discussed in [32, 33] and presented in Table 1, in all calculations we raised the reaction energy by a value negligible for our consideration up to $E_{\mathrm{kin}} = 14.4$ MeV.

The mass distribution $M^*_{^{12}\mathrm{C}}$ (20) of the excited carbon nucleus is shown in Figure 3, where the blue arrows indicate the mass values corresponding to the resonant states of the carbon-12 nucleus (see Table 1) and their appearance probabilities within the framework of the quasi-classical scattering investigated in the model. As can be seen, these probabilities vary significantly within the ensemble of single-scattering events, which can be schematically represented as

$$\begin{aligned} n + {}^{12}\mathrm{C} \to n + ({}^4\mathrm{He} + {}^8\mathrm{Be}) \to (n + {}^4\mathrm{He}) + {}^8\mathrm{Be} \\ \to (n' + {}^4\mathrm{He}') + {}^8\mathrm{Be} \to n' + {}^{12}\mathrm{C}^*. \end{aligned} \tag{23}$$

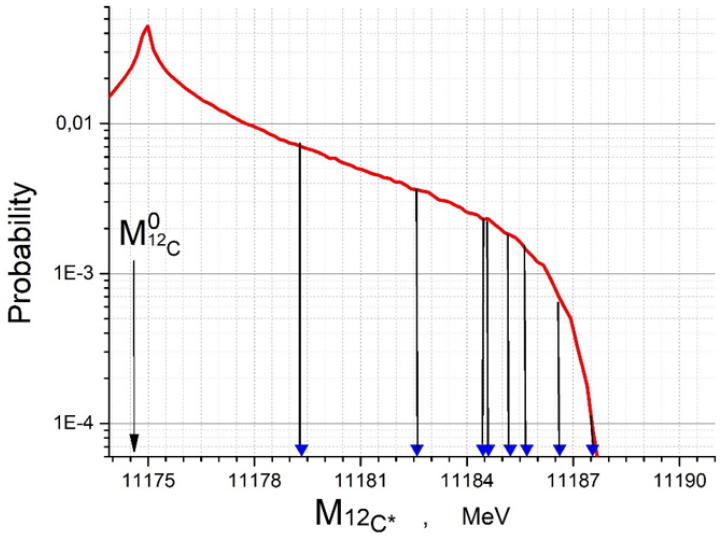


Figure 3. Monte Carlo distribution for the invariant mass $M^*_{^{12}\mathrm{C}}$ (20), obtained as a result of elastic scattering of a neutron on a cluster with the nucleon composition ^{4}He (see (23)). Here and below, the length of each blue arrow is equal to the event occurrence probability, and the arrow itself points to the values numerically matching the resonant ones (see Table 1).

The kinetic energy distribution of the neutron n' after its scattering by the ^{4}He cluster is shown in Figure 4. It clearly shows the potential for n' to participate in scattering by the second cluster of the ^{12}C nucleus, that is, by the ^{8}Be cluster. This process is discussed in Section 3.

Table 1. Resonant masses $M^*_{^{12}\mathrm{C}}$ and corresponding excitation energies $\varepsilon^*_{^{12}\mathrm{C}}$ for the ^{12}C nucleus [32, 33]. Refs. [34–42] correspond to both the $\varepsilon^*_{^{12}\mathrm{C}}$ values and the probability values in Figure 11.

$\varepsilon^*_{^{12}\mathrm{C}}$, MeV	$M^*_{^{12}\mathrm{C}}$, MeV	σ_i [mb]	Exp. Data (see Figure 11), Refs.
4.44	11179.301	210 ± 15	[35, 36]
7.65	11182.516	3.50 ± 1.0	[34, 37]
9.64	11184.503	62.0 ± 6.0	[35, 38]
9.84	11184.662	9.0 ± 3.0	[39, 40]
10.30	11185.162	6.0 ± 2.0	[37, 41]
10.84	11185.706	13.0 ± 3.0	[36, 42]
11.83	11186.69	8.0 ± 2.0	[39, 36]
12.71	11187.572	15.0 ± 2.0	[35, 36]
13.35	11188.162	2.50 ± 1.0	[37, 36]

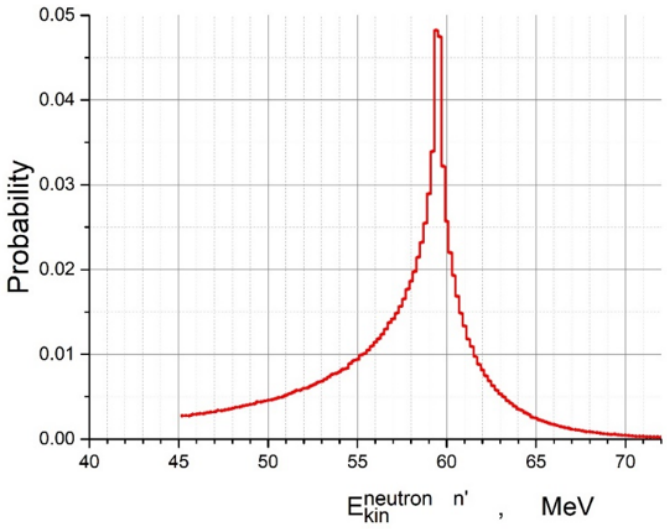


Figure 4. Monte Carlo distribution of the kinetic energy of a neutron n' after its scattering on a ^{4}He cluster (see (23)) in the potential well of the resting ^{12}C nucleus.

3. Neutron scattering on two ^{4}He and ^{8}Be clusters

3.1 Monte Carlo algorithm

The results of Section 2 indicate the need to also consider the process of successive scattering of n first on the ^{4}He cluster, and then n' on the cluster with the nucleon composition of the ^{8}Be nucleus:

$$n + {}^{12}\mathrm{C} \to n + ({}^4\mathrm{He} + {}^8\mathrm{Be}) \to (n + {}^4\mathrm{He}) + {}^8\mathrm{Be} \to$$

$$\to (n' + {}^4\mathrm{He}') + {}^8\mathrm{Be} \to {}^4\mathrm{He}' + (n' + {}^8\mathrm{Be}) \to$$

$$\to {}^4\mathrm{He}' + (n'' + {}^8\mathrm{Be}') \to n'' + ({}^4\mathrm{He}' + {}^8\mathrm{Be}') \to n'' + {}^{12}\mathrm{C}^*. \qquad (24)$$

According to scheme (24), the excited carbon nucleus consists of elastically scattered ^{4}He$'$ and ^{8}Be$'$ clusters. Comparing (23) and (24), we can see that in our study, process (23) is the first part of process (24). This simplifies the algorithm for scattering the neutron n' on the second cluster also because we again (as in Section 2.1) assume that the other (in this case, the first) cluster has no effect on this scattering process.

Thus, at the beginning of the algorithm presented in Section 2.1, in the laboratory frame K_L we had the momentum $\vec{p}_n^{\,\mathrm{Lab}}$ of the neutron n, the momentum $\vec{p}_{^4\mathrm{He}}^{\,\mathrm{Lab}}$ and the mass $m_{^4\mathrm{He}}$ of the ^{4}He cluster, the experimental [24] angular distribution (Figure 1) for elastic $n-{}^4$He scattering in the center-of-mass frame of the neutron n and the ^{4}He cluster, and as a result we obtained the momentum $\vec{p}_{n'}^{\,\mathrm{Lab}}$ and the energy $E_{n'}^{\mathrm{Lab}}$ of the scattered neutron n', the momentum $\vec{p}_{^4\mathrm{He}'}^{\,\mathrm{Lab}}$ and the energy $E_{^4\mathrm{He}'}^{\mathrm{Lab}}$ of the scattered ^{4}He$'$ cluster.

Due to the independence of scattering on clusters, we can now simply repeat the algorithm of Section 2.1, making the appropriate substitutions. Namely, at the beginning of the scattering algorithm on the second cluster, we have the momentum $\vec{p}_{n'}^{\,\mathrm{Lab}}$ and the energy $E_{n'}^{\mathrm{Lab}}$ of the neutron n' (already scattered on the first cluster ^{4}He), the momentum components (2) $p_{^8\mathrm{Be}\,x(y,z)}^{\mathrm{Lab}}$ and the energy (3) $E_{^8\mathrm{Be}}$ of the cluster with the nucleon composition ^{8}Be, as well as the angular distribution (Figure 2) for elastic $n'-{}^8$Be scattering in the center-of-mass system of the neutron n' and the cluster ^{8}Be.

As a result of repeating the algorithm of Section 2.1, we will have the momentum $\vec{p}_{n''}^{\,\mathrm{Lab}}$ and the energy $E_{n''}^{\mathrm{Lab}}$ of the rescattered neutron n'' (that is, the neutron already scattered on the first ^{4}He and second ^{8}Be clusters), the momentum $\vec{p}_{^8\mathrm{Be}'}^{\,\mathrm{Lab}}$ and the energy $E_{^8\mathrm{Be}'}^{\mathrm{Lab}}$ of the cluster ^{8}Be$'$ that has already experienced elastic scattering on a neutron. This will allow us to calculate the energy, momentum, and mass of the excited carbon nucleus using formulas (18)–(20), where, however, the energy of the unscattered cluster $E_{^8\mathrm{Be}}$ (3) should be replaced by the energy $E_{^8\mathrm{Be}'}^{\mathrm{Lab}}$ of the cluster ^{8}Be$'$ that has experienced scattering on the neutron n'.

According to the described algorithm, 10^6 Monte Carlo events were generated, in each of which the value (21) was calculated, where, however, $E_{n'}^{\mathrm{Lab}}$ was replaced by $E_{n''}^{\mathrm{Lab}}$, and it was found that the inequality $\Psi < 10^{-10}$ was satisfied, which again demonstrated the high accuracy of fulfillment of the laws of conservation of energy and momentum (see (19)) when calculating the process $n + {}^{12}\mathrm{C} \to n'' + {}^{12}\mathrm{C}^*$ (see (24)).

3.2 Results

The mass distribution of $M_{^{12}\mathrm{C}}^*$, corresponding to process (24), is shown in Figure 5. These values $M_{^{12}\mathrm{C}}^* < M_{^{12}\mathrm{C}}^0$ arise from our semiclassical analysis, where a ^{8}Be cluster does not participate in the scattering of a neutron by a ^{4}He cluster. Therefore, these values demonstrate the ability of a neutron not only to transfer energy to the target cluster but also to remove energy from it. This property of the neutron could be highly fruitful when considering thermonuclear fusion—specifically the transition from the α-gas Hoyle state [32] to the ground (or first

excited) state of the carbon nucleus transition in the presence of an external neutron. However, this requires a detailed analysis that lies far beyond the scope of the present study.

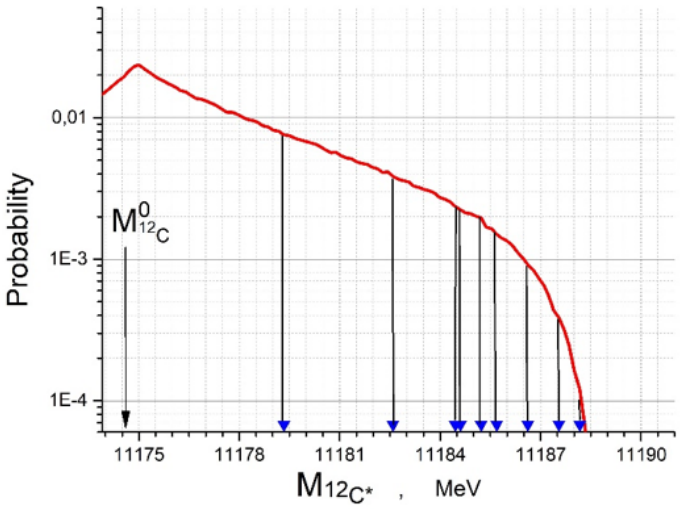


Figure 5. The same as in Figure 3, but for sequential elastic scattering of a neutron on clusters with the nucleon composition of ^{4}He and ^{8}Be (see (24), (20), Table 1, and Sect.3.1).

The kinetic energy distribution of the neutron n'' after its double scattering by two clusters with the nucleon composition ^{4}He and ^{8}Be (see (24)) is shown in Figure 6. It clearly demonstrates the potential for n'' to participate in scattering by other ^{12}C nuclei. This result may also be of interest for the chain process of thermonuclear fusion.

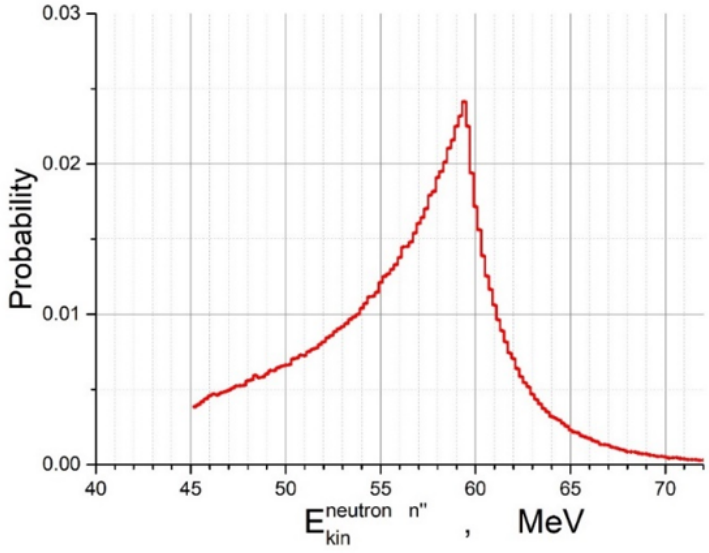


Figure 6. Monte Carlo distribution of the kinetic energy of the neutron n'' after its successive scattering on the clusters ^{4}He and ^{8}Be (see (24)) in the potential well of the resting ^{12}C nucleus.

4. Neutron scattering on two ^{4}He clusters

In this section, we will consider the sequential scattering of a neutron by two ^{4}He clusters within the cluster (^{4}He $+^4$ He $+^4$ He) structure of the ^{12}C nucleus:

$$n + {}^{12}\mathrm{C} \to n + ({}^4\mathrm{He} + {}^4\mathrm{He} + {}^4\mathrm{He}) \to (n + {}^4\mathrm{He}) + ({}^4\mathrm{He} + {}^4\mathrm{He}) \to$$

$$\to (n' + {}^4\mathrm{He}') + ({}^4\mathrm{He} + {}^4\mathrm{He}) \to n' + ({}^4\mathrm{He}' + {}^4\mathrm{He} + {}^4\mathrm{He}) \to$$

$$\to (n' + {}^4\mathrm{He}) + ({}^4\mathrm{He}' + {}^4\mathrm{He}) \to (n'' + {}^4\mathrm{He}') + ({}^4\mathrm{He}' + {}^4\mathrm{He}) \to$$

$$\to n'' + ({}^4\mathrm{He}' + {}^4\mathrm{He}' + {}^4\mathrm{He}) \to n'' + {}^{12}\mathrm{C}^*. \tag{25}$$

Within our approximation, these two scattering events occur independently. Therefore, in effect, each of these two scatterings follows the algorithm outlined in Section 2.1, but instead of the unscattered ^{8}Be cluster, one should consider the third ^{4}He cluster on which the neutron also does not scatter. The kinematic characteristics of this cluster are calculated similarly to formulas (1)–(3). Namely, both scattered ^{4}He clusters are on the mass shell. Therefore, after generating their momentum components $p^{\mathrm{Lab}}_{\mathrm{He}_1\,x(y,z)}$ and $p^{\mathrm{Lab}}_{\mathrm{He}_2\,x(y,z)}$ according to formula (1), the energies of the first E_{He_1} and second E_{He_2} clusters were found, and then the energy E_{He_3} for the third ^{4}He cluster was determined by the formula

$$E_{\mathrm{He}_3} = M^0_{^{12}\mathrm{C}} - E_{\mathrm{He}_1} - E_{\mathrm{He}_2}. \tag{26}$$

The value E_{He_3} obtained in this way was then used to calculate the energy of the excited ^{12}C* nucleus using a formula similar to (18):

$$E^{*\,\mathrm{Lab}}_{^{12}\mathrm{C}} = E^{\mathrm{Lab}}_{\mathrm{He}'_1} + E^{\mathrm{Lab}}_{\mathrm{He}'_2} + E_{\mathrm{He}_3}. \tag{27}$$

The mass of the excited ^{12}C* nucleus was calculated using formulas (19)–(20). Following the described algorithm, 10^6 Monte Carlo events were generated, in each of which an additional test was performed to verify the correctness of the software implementation of the algorithm, i.e., checking the fulfillment of condition (22).

The simulation results are presented in Figure 7, which clearly shows an increase in the excitation mass interval and, consequently, the number of resonance masses (see Table 1, Figures 3, 5) falling within this interval. Figure 8 demonstrates an increase in the fraction of low-energy scattered neutrons with an increasing number of scatterings.

5. Neutron scattering on three ^{4}He clusters

Finally, let us consider the sequential scattering of a neutron by all three ^{4}He clusters within the cluster (^{4}He $+^4$ He $+^4$ He) structure of the ^{12}C nucleus. Within our approximation, all three of these scatterings occur independently:

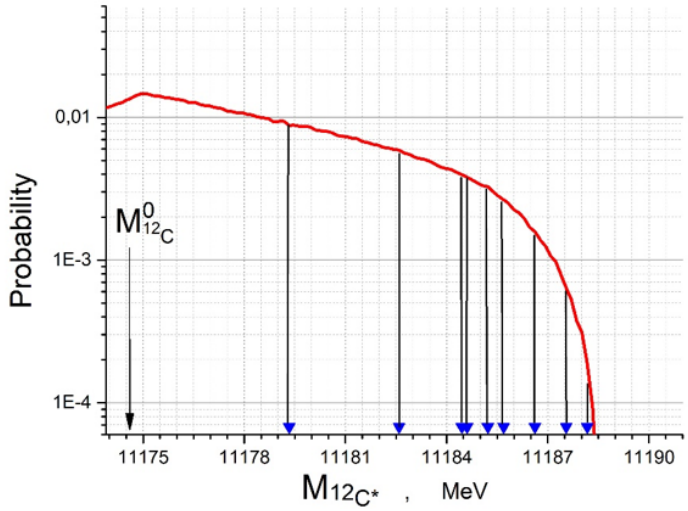


Figure 7. The same as in Figure 3, but for sequential elastic scattering of a neutron on two ^{4}He clusters (see (25), Table 1, and Sect. 4).

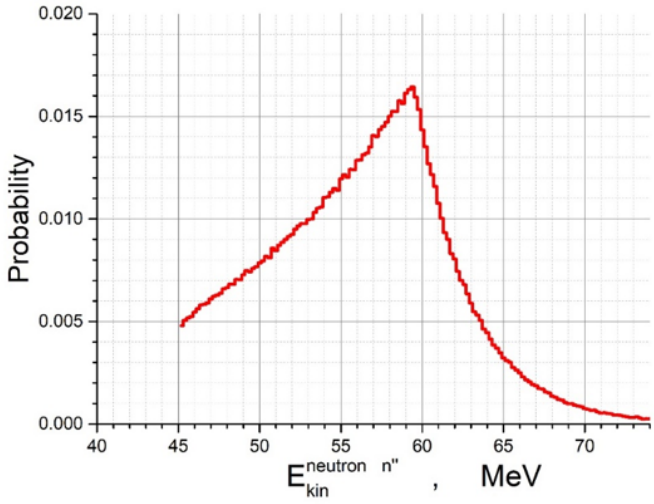


Figure 8. Monte Carlo distribution of the kinetic energy of the neutron n'' after its successive scattering on two ^{4}He clusters (see (25)) in the potential well of the resting ^{12}C nucleus.

$$n + {}^{12}\mathrm{C} \to n + ({}^4\mathrm{He} + {}^4\mathrm{He} + {}^4\mathrm{He}) \to (n + {}^4\mathrm{He}) + ({}^4\mathrm{He} + {}^4\mathrm{He}) \to$$

$$\to (n' + {}^4\mathrm{He}') + ({}^4\mathrm{He} + {}^4\mathrm{He}) \to n' + ({}^4\mathrm{He}' + {}^4\mathrm{He} + {}^4\mathrm{He}) \to$$

$$\to (n' + {}^4\mathrm{He}) + ({}^4\mathrm{He}' + {}^4\mathrm{He}) \to (n'' + {}^4\mathrm{He}') + ({}^4\mathrm{He}' + {}^4\mathrm{He}) \to$$

$$\to n'' + ({}^4\mathrm{He}' + {}^4\mathrm{He}' + {}^4\mathrm{He}) \to (n'' + {}^4\mathrm{He}) + ({}^4\mathrm{He}' + {}^4\mathrm{He}') \to$$

$$\to (n''' + {}^4\mathrm{He}') + ({}^4\mathrm{He}' + {}^4\mathrm{He}') \to n''' + ({}^4\mathrm{He}' + {}^4\mathrm{He}' + {}^4\mathrm{He}') \to$$

$$\to n''' + {}^{12}\mathrm{C}^*. \tag{28}$$

Therefore, each neutron-cluster scattering was generated according to the algorithm outlined in Section 4.1. However, the conservation of energy and momentum allows only two of the three clusters to be on the mass shell. Thus, in the rest frame of the ^{12}C target (i.e., in the Laboratory frame) prior to the neutron-cluster scattering and after the generation of the momentum components $p^{\rm Lab}_{{\rm He}_1\,x(y,z)}$ and $p^{\rm Lab}_{{\rm He}_2\,x(y,z)}$ of the first and second clusters, the momentum components and the energy of the third cluster were determined from the conservation of momentum and energy using the formulas:

$$p^{\rm Lab}_{{\rm He}_3\,x(y,z)} = -\,p^{\rm Lab}_{{\rm He}_1\,x(y,z)} - \,p^{\rm Lab}_{{\rm He}_2\,x(y,z)}, \qquad E_{{\rm He}_3} = M^0_{^{12}{\rm C}} - E_{{\rm He}_1} - E_{{\rm He}_2}. \tag{29}$$

After calculating the invariant mass of the third cluster

$$m_{{\rm He}_3} = \sqrt{\left(E_{{\rm He}_3}\right)^2 - \left(p^{\rm Lab}_{{\rm He}_3\,x}\right)^2 - \left(p^{\rm Lab}_{{\rm He}_3\,y}\right)^2 - \left(p^{\rm Lab}_{{\rm He}_3\,z}\right)^2},$$

the generation of neutron-cluster scattering proceeded according to the algorithm of Section 4. However, instead of formulas (18) and (28), formula

$$E^{*\,\rm Lab}_{^{12}{\rm C}} = E^{\rm Lab}_{{\rm He}'_1} + E^{\rm Lab}_{{\rm He}'_2} + E^{\rm Lab}_{{\rm He}'_3} \tag{30}$$

was used. Then the mass of the excited ^{12}C* nucleus was calculated using formulas (19)–(20). In each Monte Carlo event, the fulfillment of condition (22) was verified.

According to the algorithm described in Sect. 5, 10^6 Monte Carlo events were generated, in each of which the value (21) was calculated, where, however, $E^{\rm Lab}_{n'}$ was replaced by $E^{\rm Lab}_{n'''}$, and it was found that the inequality $\Psi < 10^{-10}$ was satisfied.

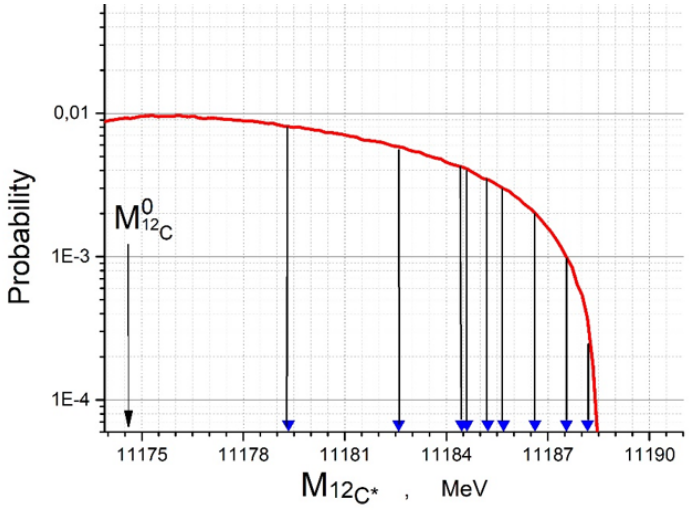


Figure 9. The same as in Figure 3, but for sequential elastic scattering of a neutron on three ^{4}He clusters (see (28), Table 1, and Sect.5).

The simulation results for process (28) are presented in Figures 9 and 10. A comparison of Figures 9 and 10 with Figures 3, 5, 7 and Figures 4, 6, 8, respectively,

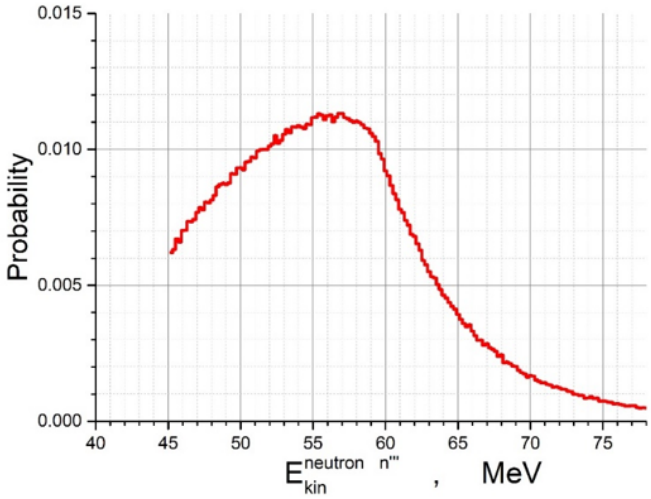


Figure 10. Monte Carlo distribution of the kinetic energy of the neutron n''' after its successive scattering on three ^{4}He clusters (see (28)) in the potential well of the resting ^{12}C nucleus.

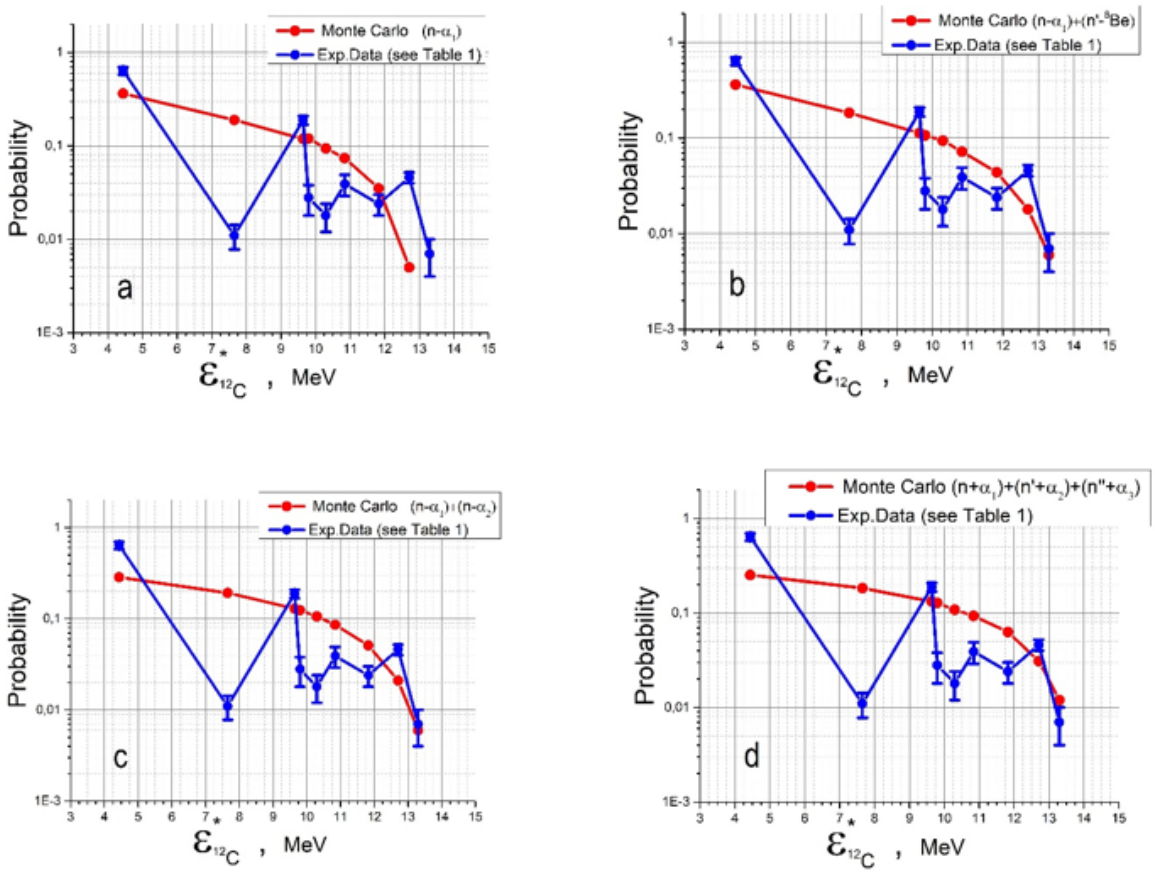


Figure 11. Level population probabilities of ^{12}C* as a function of excitation energy $\varepsilon^*_{^{12}C}$ for inelastic 14.4 MeV neutron scattering. Blue circles represent experimental values [34–42], extracted as net peak cross sections with the non-resonant background subtracted (see Table 1). Red circles show the corresponding Monte Carlo distribution for the same excitation energies as $M^*_{^{12}C} - M^0_{^{12}C}$. Figures a, b, c, and d correspond to Monte Carlo reactions (23), (24), (25), and (28), respectively.

demonstrates an expected clear trend toward an increase in the average mass of ^{12}C* and a decrease in the average energy carried away by the scattered neutron. At the same time, Figures 3, 5, 7, and 9 predict a distinctly different probability of appearance for each resonance when a neutron is scattered by different clusters

and by a different number of clusters.

6. Conclusion

This paper studies the interaction between a neutron with a kinetic energy of 14 MeV and a target carbon-12 nucleus at rest.

As noted in Section 1, in the range of excitation energies of the ^{12}C nucleus from the Hoyle state ($\varepsilon^*_{^{12}\mathrm{C}} = 7.65$ MeV) and higher, up to 13.35 MeV and further to 16–20 MeV, and especially in the region of closely lying resonances, knowledge about the α-cluster configuration and reaction cross sections is probabilistic and model-dependent. In determining cross sections, this creates a discrepancy of 30–50% and higher [10] between values in different nuclear databases. For a possible solution to the problem, this work proposes to investigate a probable relationship between the population of excitation levels of the ^{12}C nucleus and the scattering of the projectile neutron on various nuclear clusters.

As a first step, that is, as a first approximation, we use a rough picture of the nucleus as a potential well in which the cluster structures (^{4}He $+^4$ He $+^4$ He) or (^{4}He $+^8$ Be) move independently, scattering the neutron according to the laws of quantum scattering (Figures 1, 2). In such a treatment, the nuclear mass represents the invariant mass of the cluster system of which the nucleus consists. In energy-momentum space, the Monte Carlo model calculates processes (23)–(25), (28). In the neutron–cluster center-of-mass system, the scattering angle was generated according to the data presented in Figures 1, 2.

The simulation results are shown in Figures 3–10, which demonstrate that scattering on different clusters leads to different distributions for the invariant mass of the ^{12}C nucleus (Figures 3, 5, 7, 9) and different kinetic energy distributions of the neutron (Figures 4, 6, 8, 10) that underwent scattering on the clusters and exited the nuclear potential well with a depth of 45 MeV.

Figure 11 shows a comparison between the model-calculated invariant mass and the experimentally calculated population of excitation levels of the ^{12}C nucleus [34–42]. All distributions are normalized to unity. Due to the large number of simulated events (10^6), the statistical uncertainties of the Monte Carlo simulation are smaller than the size of the red points shown in Figure 11. Despite a very rough approximation of the nucleus as a potential well with independent motion of clusters, qualitative consistency is observed in Figure 11. A strong discrepancy occurs at those values of $\varepsilon^*_{^{12}\mathrm{C}}$ where there is a strict quantum suppression for the formation of an excited state (for example, the Hoyle state at $\varepsilon^*_{^{12}\mathrm{C}} = 7.654$ MeV) or, conversely, a pronounced (quadrupole) nuclear collectivity ($\varepsilon^*_{^{12}\mathrm{C}} = 4.439$ MeV). However, it is interesting that with increasing $\varepsilon^*_{^{12}\mathrm{C}}$, a certain generality is observed on average in describing the evolution of the process.

Furthermore, even the used rough approximation of the ^{12}C nucleus as a group of independent clusters demonstrates the dependence of the Monte

Carlo distribution on the type and number of neutron–cluster scatterings. This inspires optimism for further investigation of the correlations between the type of intranuclear scattering and the population of excitation levels of the ^{12}C nucleus represented in a more realistic model, where the overlap of the de Broglie waves of α-particles is taken into account.

It is indeed true that in the independent α-particle model used, the incident neutron "sees" first an α-particle with a radius of 1.68 fm, rather than a nucleus with a radius of ≈ 2.5 fm. A different picture emerges in the model that takes into account the overlap of wave functions and strong correlation of α-particles in the quadrupole state ($\varepsilon^*_{^{12}C} = 4.44$ MeV), where the neutron "sees" the entire disk of the nucleus with a radius of ≈ 2.5 fm, i.e., the neutron sees a target 2.1 times larger, since the ratio of the cross-sectional areas of the nucleus and the α-particle is 2.1.

Therefore, when transitioning from the independent α-particle model to the model taking into account the overlap of their wave functions, in Figure 11 at $\varepsilon^*_{^{12}C} = 4.44$ MeV it is natural to expect an increase in the theoretical point by ≈ 2 times until it matches the experimental value (for level population), which in Figure 11 is larger by ≈ 2 times.

Both the ground state of the ^{12}C nucleus and the Hoyle state have zero spin. Therefore, for the formation of the Hoyle state, the incident neutron must impinge with a zero impact parameter on a system of three α-particles aligned along the neutron momentum. This is a very rare event, hence its cross section is small. Otherwise, the ^{12}C nucleus would acquire angular momentum, and the nuclear spin would be non-zero. Then one of the states with a much larger spin value would be formed.

Here, the contradiction for the described crude model of independent α-particles is that a zero impact parameter in elastic scattering implies the maximum value of $\varepsilon^*_{^{12}C}$ at the minimum spin of the $^{12}C^*$ nucleus. Whereas from Figure 11, the well-known fact is visible that states with the maximum value of $\varepsilon^*_{^{12}C}$ have non-zero spin. If, however, one assumes the alignment of α-particles along the neutron momentum line and at the same time takes into account the overlap of α-particle wave functions, the elastic scattering of a neutron can be considered as occurring on all three α-particles as a single whole. Then (see Section 1) the fraction of transferred energy, i.e., $\varepsilon^*_{^{12}C}$, will be smaller at zero spin of $^{12}C^*$. In this case (see Section 1), scattering on several α-particles, randomly distributed in the volume of the nucleus, can yield a larger value for both the spin and the excitation energy $\varepsilon^*_{^{12}C}$.

The above highly approximate, crude reasoning demonstrates the clear advantage of treating the process within the framework of the wave nature of the α-cluster structure. Here, an important role begins to be played by the well-known Ikeda concept (Ikeda diagram) [2], according to which, at least in light nuclei, cluster structures begin to manifest themselves vividly near or above the decay threshold into these cluster structures, which, during the characteristic lifetime of the resonance state, would behave as sufficiently individual objects governed by the equations of motion characteristic of this process and being solved.

Perhaps the solution to this problem should be sought in the Quark Cluster Model [43], which bridges the cluster approach with the quark level, describes the transition from meson exchange to quark degrees of freedom, and satisfies the requirements of the Pauli exclusion principle under strong cluster overlap.

Acknowledgments

Author V.V.L. expresses gratitude to J. Morillo for assistance. The work was funded by the State Budget of Uzbekistan through Uzbekistan Academy of Sciences.

References

[1] K. Wildermuth, Y.C. Tang, A Unified Theory of the Nucleus (Vieweg, Braunschweig, 1977) 389 p. [*CrossRef*]
[2] C. Beck, Clusters in Nuclei, Lecture Notes in Physics (Springer: Berlin, 2010) 315 p. [*CrossRef*]
[3] K. Ikeda, H. Horiuchi, S. Saito, Progress of Theoretical Physics Supplement **68** (1980) 1–28. [*CrossRef*]
[4] H. Horiuchi, K. Ikeda, International Review of Nuclear Physics **4** (1986) 1.
[5] W. von Oertzen, M. Freer, Y. Kanada-En'yo, Physics Reports **432** (2006) 43–113. [*CrossRef*]
[6] K. Ikeda, N. Takigawa, H. Horiuchi, Progress of Theoretical Physics Supplement **E68** (1968) 464–475. [*CrossRef*]
[7] M. Freer, H.O.U. Fynbo, Progress in Particle and Nuclear Physics **78** (2014) 1–23. [*CrossRef*]
[8] T.K. Wheldon, Journal of Physics: Conference Series **639** (2015) 012003. [*CrossRef*]
[9] M. Freer et al., Reviews of Modern Physics **90** (2018) 035004. [*CrossRef*]
[10] E. Belfiore, M. B. Mosbah, R. Antoni, Proceedings of the International Conference on Mathematics and Computational Methods Applied to Nuclear Science and Engineering (Denver, 2025) 1656–1664.
[11] J.M. Blatt, V.F. Weisskopf, Theoretical Nuclear Physics, John Wiley & Sons, New York, 1952. [*Web link*]
[12] P.E. Hodgson, Reports on Progress in Physics **34** (1971) 765–819. [*CrossRef*]
[13] D.R. Tilley, H.R. Weller, G.M. Hale, Nuclear Physics A **541** (1992) 1–104.
[14] S. Fernbach, R. Serber, T.B. Taylor, Physical Review **75** (1949) 1352–1355. [*CrossRef*]
[15] P.E. Hodgson, The Optical Model of Elastic Scattering (Clarendon Press, Oxford, 1963) 211 p.
[16] J.J. Krauth et al., Nature **589** (2021) 527–531. [*CrossRef*]
[17] I. Angeli, K.P. Marinova, Atomic Data and Nuclear Data Tables **99** (2013) 69–95. [*CrossRef*]
[18] P.E. Hodgson, Nuclear Reactions and Nuclear Structure (Clarendon Press, Oxford, 1971) 661 p.

[19] J.K. Dickens, Oak Ridge National Laboratory Report ORNL-6463 (1988). [*Web link*]
[20] S. Agostinelli et al., Nuclear Instruments and Methods in Physics Research Section A **506** (2003) 250–303. [*CrossRef*]
[21] F.P. Brady et al., Physical Review C **9** (1974) 1784. [*CrossRef*]
[22] R.P. Devito et al., Physical Review C **28** (1983) 1480.
[23] B.K. Park et al., Physical Review C **44** (1991) 1524.
[24] IAEA, EXFOR Nuclear Reaction Data Library, Entry 22312. [*Web link*]
[25] A.G. Sitenko, Theory of Nuclear Reactions (World Scientific, Singapore, 1990) 636 p. [*CrossRef*]
[26] I. Ahmad, Annals of Physics **95** (1975) 548.
[27] N.S. Chant, P.G. Roos, Physical Review C **15** (1977) 57–68. [*CrossRef*]
[28] M. Freer, Reports on Progress in Physics **70** (2007) 2149–2210. [*CrossRef*]
[29] A.I. Abramov, Fundamentals of Nuclear Physics (Energoatomizdat, Moscow, 1983) 256 p. (In Russian).
[30] J.R. Lamarsh, A.J. Baratta, Introduction to Nuclear Engineering, 3rd ed. (Prentice Hall, Upper Saddle River, NJ, 2001) 783 p. [*Web link*]
[31] T.A. Carey et al., Physical Review C **29** (1984) 1273–1288. [*CrossRef*]
[32] T.K. Wheldon, Journal of Physics: Conference Series **639** (2015) 012003. [*CrossRef*]
[33] J.H. Kelley, J.E. Purcell, C.G. Sheu, Nuclear Physics A **968** (2017) 71–253. [*CrossRef*]
[34] G. Haouat et al., Nuclear Science and Engineering **65** (1978) 331–346. [*CrossRef*]
[35] M. Baba et al., Journal of Nuclear Science and Technology **27** (1990) 601–616. [*CrossRef*]
[36] G.L. Morgan, J.K. Dickens, Production of Low Energy Gamma Rays by Neutron Interactions with Fluorine for Incident Neutron Energies Between 0.1 and 20 MeV, Oak Ridge National Laboratory Report ORNL-TM-4823, 1975. [*Web link*]
[37] IAEA Nuclear Data Section, EXFOR: Experimental Nuclear Reaction Data, International Atomic Energy Agency (IAEA). [*Web Link*]
[38] S. Meigo, Journal of Nuclear Science and Technology **31** (1994) 1221.
[39] M. Itoh et al., Physical Review C **84** (2011) 054308. [*CrossRef*]
[40] M. Freer, H.O.U. Fynbo, Progress in Particle and Nuclear Physics **78** (2014) 1–23. [*CrossRef*]
[41] H.O.U. Fynbo et al., Nature **433** (2005) 136–139. [*CrossRef*]
[42] K. Shibata et al., Journal of Nuclear Science and Technology **48** (2011) 1–30. [*CrossRef*]
[43] A.J. Buchmann, A. Faessler, A. Arima, Nuclear Physics A **526** (1991) 636.